Zhang and Sabharwal
J Wireless Com Network (2023) 2023:29
https://doi.org/10.1186/s13638-022-02199-z

EURASIP Journal on Wireless Communications and Networking

RESEARCH Open Access

Analysis of scalable channel estimation in FDD massive MIMO

Xing Zhang* and Ashutosh Sabharwal

*Correspondence:
ee.xing.zhang@gmail.com

Department of Electrical and Computer Engineering, Rice University, Houston, USA

Abstract

One of the key ideas for reducing downlink channel acquisition overhead for FDD massive MIMO systems is to exploit a combination of two assumptions: (i) the dimension of channel models in propagation domain may be much smaller than the next-generation base-station array sizes (e.g., 64 or more antennas), and (ii) uplink and downlink channels may share the same low-dimensional propagation domain. Our channel measurements demonstrate that the two assumptions may not always hold, thereby impacting the predicted performance of methods that rely on the above assumptions. In this paper, we analyze the error in modeling the downlink channel using uplink measurements, caused by the mismatch from the above two assumptions. We investigate how modeling error varies with base-station array size and provide both numerical and experimental results. We observe that modeling error increases with the number of base-station antennas, and channels with larger angular spreads have larger modeling error. Utilizing our modeling error analysis, we then investigate the resulting beamforming performance rate loss. Accordingly, we observe that the rate loss increases with the number of base-station antennas, and channels with larger angular spreads suffer from higher rate loss.

Keywords: Massive MIMO, FDD, Channel estimation, Propagation domain

1 Introduction

Massive multi-input and multi-output (MIMO) [1–5] uses many antennas at the base-station to improve communication in diverse ways [6–13]. However, due to the large number of antennas, the key challenge in enabling FDD[1] massive MIMO is that the downlink channel acquisition overhead scales with the base-station array size. Several recent works have proposed methods to exploit lower dimensionality of the channel with propagation domain channel characterizations to address this channel estimation challenge [14–25]. The proposed schemes leverage two key assumptions: (i) the cardinality of the alternate channel characterizations is much smaller than and independent of the number of base-station antennas, and (ii) uplink and downlink channels share the same low-dimensional propagation characteristics. With the two assumptions, the downlink channel can be parameterized by a few coefficients and an estimate of these coefficients can be obtained from uplink channel.

[1] Frequency-division Duplex

However, our recent channel measurement-based work [26] demonstrated that the two assumptions may not hold exactly. Our two main findings based on measured channels were: (i) dominant angles do not capture all the channel power, even though a significant fraction can be captured, and (ii) uplink and downlink dominant angles are not exactly the same, even though the angle correlation can be high. In short, the two assumptions can be good assumptions but not guaranteed to hold unilaterally. In the same paper [26], we had also proposed a directional training scheme, where the base-station trains downlink channel with estimated uplink dominant angles and, in essence, relies on approximation and reciprocity of channel in the propagation domain. However, the mismatch between the assumed channel model and the actual channel model can lead to downlink beamforming performance loss. Therefore, to quantify the possible performance gaps of training downlink channel in the propagation domain using uplink channel measurements, it is important to revisit the two key assumptions on FDD massive MIMO channels and quantify the loss in performance due to each of these assumptions.

In this paper, we focus on the fundamentals to analyze the *modeling error* in approximating downlink channel with uplink dominant angles in the propagation domain for FDD massive MIMO channels. With the proposed error analysis, we aim to answer two questions:

Q1 How does the modeling error scale with the number of base-station antennas?
Q2 How does the modeling error vary in different propagation environments?

Answering Question 1 is important to quantify the performance scalability in the large-array regime, which will have implications as the number of antennas is scaled in upcoming generations of massive MIMO systems. Similarly, answering Question 2 is important to understand the performance dependency on different channel scenarios. In particular, we will show that the channel angle spread is the important channel parameter that impacts modeling error.

Based on the modeling error analysis, we investigate the impact of downlink beamforming performance in training downlink channel with estimated uplink dominant angles. We quantify the downlink beamforming rate loss and study scalability with the base-station array size and dependency on the channel angle spread for the rate loss. Overall, our main contributions in this paper are as follows:

1 We define the modeling error to quantify the normalized error of approximating downlink channel with uplink dominant angles. There are two factors that affect modeling error. First is that dominant angles do not capture all the channel power; we label this error as *approximation error*. Second is that uplink and downlink dominant angles are not exactly the same; we label this as *mismatch error*. The two errors contribute additively toward the overall modeling error.
2 We employ the 3GPP spatial channel model [27] to investigate scalability with the base-station array size and dependency on the channel angle spread for modeling error. Using the channel model, we conduct extensive numerical simulations to examine modeling error in the finite array regime. We observe that modeling error

increases with the number of base-station antennas, and a larger channel angle spread yields a larger modeling error.

3 We further validate our numerical observations utilizing our measured channels. The main finding is that our experimental results match the observations from the numerical results. We find that modeling error increases with the number of base-station antennas, from 2% as the average modeling error when the base-station is equipped with 4 antennas, to 28% as the average modeling error when the base-station is equipped with 64 antennas for non-line-of-sight channels. The other observation is that larger angle spread in angle of arrivals leads to larger modeling error, with average modeling error as 28% for non-line-of-sight channels, compared to the average modeling error as 13% for line-of-sight channels when the base-station is equipped with 64 antennas.

4 To investigate the performance impact of modeling error, we also quantify the resulting downlink beamforming rate loss. Similar to modeling error, we provide both numerical and experimental results. From both numerical and experimental results, we observe that the rate loss increases with the number of base-station antennas, and more distributed power channel will bring in larger rate loss. Also, even though the rate loss increases with the number of base-station antennas, we find out resulted beamforming rate still increases with array size. So we conclude that beamforming based on scalable channel estimation schemes that exploit the propagation domain, e.g., directional training [26], still benefits from the array gain in FDD massive MIMO.

As a future extension, the proposed approach can be used to understand the impact of modeling error on other methods [14–25].

The rest of the paper is outlined as follows. Section 2 formulates the research problem and defines the model error to analyze channel estimation errors in FDD massive MIMO. Section 3 provides both numerical and experimental results of modeling error and evaluates the performance impact of modeling error. Finally, Sect. 4 concludes this paper.

2 Methods

2.1 System model

We consider a single-cell FDD massive MIMO system where an M-antenna base-station serves K single-antenna users through downlink beamforming. With downlink channel as $\mathbf{H} \in \mathbb{C}^{K\times M}$ and beamforming weights matrix as $\mathbf{W} \in \mathbb{C}^{M\times K}$, the received signals at the mobile user can be written as

$$\mathbf{y} = \mathbf{HWx} + \mathbf{n}, \tag{1}$$

where $\mathbf{x} \in \mathbb{C}^K$ is the transmitted signals and $\mathbf{n} \in \mathbb{C}^K$ is the additive noises that follow standard complex Gaussian distribution.

To design beamforming weights $\mathbf{W}$ for effective downlink multi-user beamforming, e.g., conjugate beamforming or zero-forcing beamforming, the key step is to estimate downlink channel state information at the base-station side. Therefore, next, we first present details of FDD massive MIMO channels, including propagation domain channel

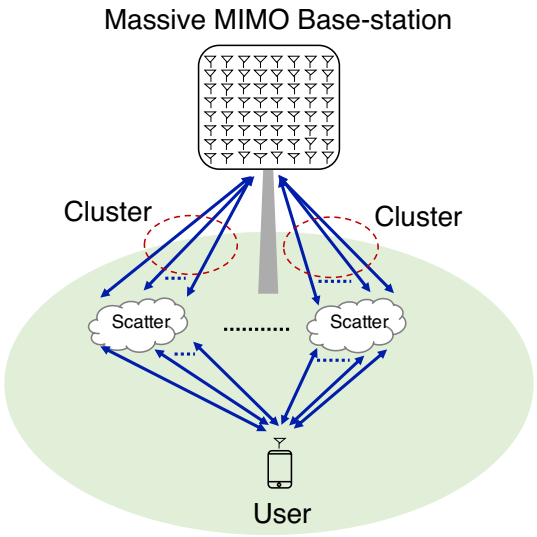

Fig. 1 Propagation paths between a massive MIMO base-station and a single-antenna user

model and measured channels, and then show potential errors of existing scalable channel estimation schemes in FDD massive MIMO.

2.2 FDD massive MIMO channels

2.2.1 Propagation domain channels

We adopt the popular geometrical ray-tracing approach and employ the 3GPP spatial channel model [27] to model FDD massive channels in the propagation domain. Note that the main propagation mechanisms include line-of-sight, reflection, diffraction, and scattering of the transmitted electromagnetic signals. In FDD mode, even though uplink and downlink transmit at different frequency bands, the frequency gap between uplink and downlink is relatively small in many cases, e.g., less than 100 MHz in sub-6 GHz FDD bands. As a result, with the proximity of the wavelengths, uplink and downlink can be approximated to undergo through the same propagation paths and have the same amplitude for each corresponding path. However, since the phase is very sensitive to wavelength difference, the phases are often modeled as uniform i.i.d. random, $U[0, 2\pi)$.

Therefore, consider the system where the base-station is equipped with an M antennas uniform plane array, consisting of M_r rows and M_c columns. We use the geometrical ray-tracing approach as illustrated in Fig. 1. First, the downlink channel with frequency f_{D} between the M-antenna base-station and a single-antenna user can be modeled as

$$\mathbf{h}_{\mathrm{D}} = \sum_{i=1}^{I} \sum_{j=1}^{J_i} \sqrt{g_{ij}} e^{j\phi_{\mathrm{Dij}}} \mathbf{a}_{f_{\mathrm{D}}}\left(\theta_{ij}, \varphi_{ij}\right), \tag{2}$$

where the channel consists of I clusters and the ith cluster consists of J_i paths; the jth path of ith cluster has power g_{ij}, independent phase $\phi_{\mathrm{Dij}} \sim U[0, 2\pi)$ and angle with elevation as θ_{ij} and azimuth as φ_{ij}. The array response vector $\mathbf{a}_f(\theta, \varphi)$ corresponding to the M_r rows and M_c columns uniform plane array is defined as

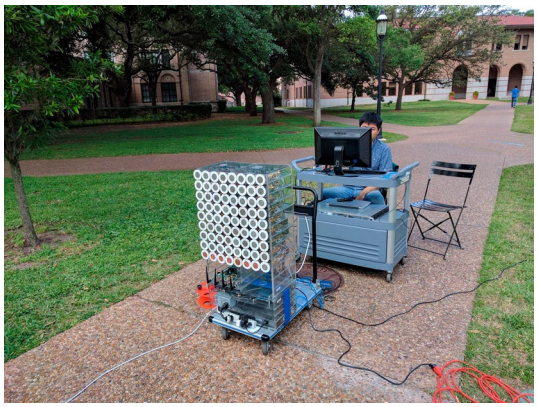

Fig. 2 Channel measurements setup with large-array base-station. The plot comes from [26]

$$\mathbf{a}_f(\theta,\varphi) = \begin{bmatrix} 1 \\ e^{j\frac{2\pi}{\lambda}d\sin\theta\cos\varphi} \\ \vdots \\ e^{j\frac{2\pi}{\lambda}d((M_r-1)\cos\theta+(M_c-1)\sin\theta\cos\varphi)} \end{bmatrix}, \tag{3}$$

where f is the received signal frequency; λ is the signal wavelength; d is the antenna spacing; θ is the elevation angle; and φ is the azimuth angle.

Then, accordingly, using the geometrical ray-tracing approach, the corresponding uplink channel operated at a different frequency band f_{U} of the same base-station user pair can be modeled as

$$\mathbf{h}_{\mathrm{U}} = \sum_{i=1}^{I}\sum_{j=1}^{J_i}\sqrt{g_{ij}}e^{j\phi_{\mathrm{Uij}}}\mathbf{a}_{f_{\mathrm{U}}}(\theta_{ij},\varphi_{ij}). \tag{4}$$

For small frequency differences, uplink and downlink channel will have the same number of clusters I and same number of paths J_i in the ith cluster. The jth path of ith cluster has the same power g_{ij} and same angles $(\theta_{ij}, \varphi_{ij})$ as downlink channel. The only different channel parameter is the phase component, with value i.i.d. in $U[0, 2\pi)$, respectively.

2.2.2 Measured channels

The measured FDD massive MIMO channels are presented in our previous work [26], with all the details explained therein. Overall, the channel dataset includes FDD massive MIMO channels corresponding to 21 non-line-of-sight and 4 line-of-sight user locations. For each user location, two 20 MHz wide-band channels, each with 52 OFDM subcarriers and separated by about 72 MHz, are measured across around 5000 time frames. Further, the base-station is equipped with an 8-row 8-column uniform plane array, as shown in Fig. 2 with plots from [26]. Overall, the entire dataset includes 52 (subcarriers) × 52 (subcarriers) × 25 (user locations)= 67600 FDD massive MIMO uplink/downlink channel instance pairs, including 56784 non-line-of-sight ones and 10816 line-of-sight ones.

2.3 Scalable channel estimation in FDD massive MIMO

To investigate the potential error of downlink channel estimation, here we focus on the single-user case only. Without loss of generality, the user downlink channel is denoted as $\mathbf{h}_{\mathrm{D}} \in \mathbb{C}^M$. Based on the propagation domain channel model, as shown in Eq. 2, downlink channel model can be rewritten as

$$\mathbf{h}_{\mathrm{D}} = \sum_{i=1}^{I} \sum_{j=1}^{J_i} \sqrt{g_{ij}} e^{j\phi_{\mathrm{Dij}}} \mathbf{a}\left(\theta_{ij}, \varphi_{ij}\right) = \mathbf{Sb}, \tag{5}$$

where

$$\mathbf{S} = \left[\mathbf{a}(\theta_{11}, \varphi_{11}) \ \cdots \ \mathbf{a}\left(\theta_{1J_1}, \varphi_{1J_1}\right) \ \cdots \ \mathbf{a}(\theta_{I1}, \varphi_{I1}) \ \cdots \ \mathbf{a}\left(\theta_{IJ_I}, \varphi_{IJ_I}\right)\right] \tag{6}$$

denotes full propagation domain and

$$\mathbf{b} = \left[\sqrt{g_{11}} e^{j\phi_{\mathrm{D11}}} \ \cdots \ \sqrt{g_{1J_1}} e^{j\phi_{\mathrm{D1J_1}}} \ \cdots \ \sqrt{g_{I1}} e^{j\phi_{\mathrm{DI1}}} \ \cdots \ \sqrt{g_{IJ_I}} e^{j\phi_{\mathrm{DIJ_I}}}\right]^T \tag{7}$$

coefficients in the propagation domain.

In scalable channel estimation schemes that exploit channel low-dimensional domain, there are two main steps. First, estimate the low-dimensional propagation domain $\hat{\mathbf{S}} \in \mathbb{C}^{M \times L}, L < M$ for downlink training, where L is the number of training vectors in the estimated domain. Second, estimate domain coefficients $\hat{\mathbf{b}} \in \mathbb{C}^L$ via downlink training and uplink feedback. After that, the downlink channel can be reconstructed as

$$\hat{\mathbf{h}}_{\mathrm{D}} = \hat{\mathbf{S}}\hat{\mathbf{b}}. \tag{8}$$

Previous works focus on domain coefficients estimation as in the second step only and assume perfect knowledge of the channel propagation domain. However, the error in propagation domain estimation $\hat{\mathbf{S}}$ also contributes to channel estimation error. Therefore, it is important to investigate the impact of propagation domain estimation error.

Since we aim to quantify the *propagation domain* modeling error—normalized error of approximating downlink channel with uplink dominant angles, next we ask and answer two questions on propagation domain estimation corresponding to the imperfectness of the two aforementioned assumptions that will affect the normalized error:

1. What will be the normalized error if utilizing dominant angles in the propagation domain instead of all angles to approximate the downlink channel?
2. What will be the extra normalized error if utilizing uplink dominant angles instead of downlink ones to approximate the downlink channel?

The answers to the questions depend on channel properties only. Therefore, to answer the questions, we seek to start from the fundamentals, i.e., FDD massive MIMO channels, to investigate the normalized error of approximating downlink channel with uplink dominant angles. We use a combination of a numerical and experimental approach. For the numerical approach, we employ the spatial channel model to

formulate modeling error and examine the scalability with the base-station array size and dependency on the channel angle spread; for the experimental approach, we further validate the observations of modeling error based on measured channels.

2.4 Modeling error definition

In this section, we characterize the normalized error of approximating downlink channel with uplink dominant propagation domain, defined as *modeling error*, by answering the two questions brought up in Sect. 2.3. Each question corresponds to one source of error, with the first one denoted as *approximation error* and the second one denoted as *mismatch error*.

For single-user case, the resulting rate with conjugate beamforming based on estimated channel $\hat{\mathbf{h}}_{\mathrm{D}} \in \mathbb{C}^M$ is

$$\begin{aligned} R\left(\hat{\mathbf{h}}_{\mathrm{D}}, \mathbf{h}_{\mathrm{D}}\right) &= \mathbb{E}\left[\log\left(1 + P\frac{\|\hat{\mathbf{h}}_{\mathrm{D}}^H \mathbf{h}_{\mathrm{D}}\|^2}{\|\hat{\mathbf{h}}_{\mathrm{D}}\|^2}\right)\right] \\ &= \mathbb{E}\left[\log\left(1 + P\underbrace{\|\mathbf{h}_{\mathrm{D}}\|^2}_{P_{\text{channel}}}\frac{\|\hat{\mathbf{h}}_{\mathrm{D}}^H \mathbf{h}_{\mathrm{D}}\|^2}{\|\hat{\mathbf{h}}_{\mathrm{D}}\|^2\|\mathbf{h}_{\mathrm{D}}\|^2}\right)\right] \end{aligned} \tag{9}$$

where P denotes the downlink transmission power for the user. From Eq. (9), maximizing rate is same as minimizing the following *normalized* error

$$E = 1 - \frac{\|\hat{\mathbf{h}}_{\mathrm{D}}^H \mathbf{h}_{\mathrm{D}}\|}{\|\hat{\mathbf{h}}_{\mathrm{D}}\|\|\mathbf{h}_{\mathrm{D}}\|}. \tag{10}$$

Note $E \in [0, 1]$, where $E = 0$ occurs when there is no channel estimation error and $E = 1$ occurs when the estimated channel is orthogonal to the actual channel, a worst-case scenario. Thus, smaller E is better.

We focus on propagation domain estimation and assume genie-aided domain coefficients training. Consider estimated propagation domain $\hat{\mathbf{S}} \in \mathbb{C}^{M\times L}, L < M$, the genie-aided estimated domain coefficients will be

$$\hat{\mathbf{b}} = \hat{\mathbf{S}}^{\dagger}\mathbf{h}_{\mathrm{D}} \tag{11}$$

based on least-square estimator, where $\hat{\mathbf{S}}^{\dagger}$ stands for the pseudo-inverse matrix of $\hat{\mathbf{S}}$. To evaluate estimated propagation domain $\hat{\mathbf{S}}$, based on Eq. 10, we consider the normalized error of estimated downlink channel utilizing the estimated propagation domain, which is formulated as

$$\begin{aligned} E(\hat{\mathbf{S}}) &= 1 - \frac{\|\hat{\mathbf{h}}_{\mathrm{D}}^H \mathbf{h}_{\mathrm{D}}\|}{\|\hat{\mathbf{h}}_{\mathrm{D}}\|\|\mathbf{h}_{\mathrm{D}}\|} \\ &= 1 - \frac{\|(\hat{\mathbf{S}}\hat{\mathbf{b}})^H \mathbf{h}_{\mathrm{D}}\|}{\|\hat{\mathbf{S}}\hat{\mathbf{b}}\|\|\mathbf{h}_{\mathrm{D}}\|} \\ &= 1 - \frac{\|(\hat{\mathbf{S}}\hat{\mathbf{S}}^{\dagger}\mathbf{h}_{\mathrm{D}})^H \mathbf{h}_{\mathrm{D}}\|}{\|\hat{\mathbf{S}}\hat{\mathbf{S}}^{\dagger}\mathbf{h}_{\mathrm{D}}\|\|\mathbf{h}_{\mathrm{D}}\|}. \end{aligned} \tag{12}$$

We aim to quantify modeling error—the normalized error of approximating downlink channel with uplink dominant propagation domain. To analyze modeling error, we need to obtain both downlink domain of low dimensionality and uplink one. In propagation domain, the low dimensionality part is constructed from array response vectors corresponding to dominant channel angles. Therefore, first, we try to construct downlink dominant propagation domain $\mathbf{S}_{\mathrm{d}} \in \mathbb{C}^{M \times L_d}, L_d \ll M$, where M is the number of antennas at the base-station and L_d is the number of dominant angles. The downlink dominant angle set is defined as

$$\left\{(\theta_{\mathrm{d}1}, \varphi_{\mathrm{d}1}), ..., \left(\theta_{\mathrm{dL_d}}, \varphi_{\mathrm{dL_d}}\right)\right\} = \arg \underset{\left\{(\theta_1,\varphi_1),...,\left(\theta_{L_d},\varphi_{L_d}\right)\right\}}{\text{minimize}} \left\|\mathbf{h}_{\mathrm{D}} - \mathbf{A}_{\mathrm{d}}\mathbf{A}_{\mathrm{d}}^{\dagger}\mathbf{h}_{\mathrm{D}}\right\|_2, \tag{13}$$

where $\mathbf{A}_{\mathrm{d}} = \left[\mathbf{a}(\theta_1, \varphi_1) \ \cdots \ \mathbf{a}\left(\theta_{L_d}, \varphi_{L_d}\right)\right]$ and $\mathbf{A}_{\mathrm{d}}^{\dagger}$ stands for the pseudo-inverse matrix of $\mathbf{A}_{\mathrm{d}}$. We extract downlink dominant angles from full downlink CSI $\mathbf{h}_{\mathrm{D}} \in \mathbb{C}^M$ utilizing maximum likelihood estimator [26]. Then, the downlink dominant propagation domain based on dominant angles is constructed as

$$\mathbf{S}_{\mathrm{d}} = \left[\mathbf{a}(\theta_{\mathrm{d}1}, \varphi_{\mathrm{d}1}) \ \mathbf{a}(\theta_{\mathrm{d}2}, \varphi_{\mathrm{d}2}) \ \cdots \ \mathbf{a}\left(\theta_{\mathrm{dL_d}}, \varphi_{\mathrm{dL_d}}\right)\right], \tag{14}$$

where $\mathbf{a}$ is the array response vector defined in Eq. (3).

Second, to construct uplink dominant propagation domain $\mathbf{S}_{\mathrm{u}} \in \mathbb{C}^{M \times L_d}$, similarly, we extract uplink dominant angles $\left\{(\theta_{\mathrm{u}1}, \varphi_{\mathrm{u}1}), ..., \left(\theta_{\mathrm{uL_d}}, \varphi_{\mathrm{uL_d}}\right)\right\}$ from full uplink CSI $\mathbf{h}_{\mathrm{U}} \in \mathbb{C}^M$. Then, the uplink dominant propagation domain is constructed as

$$\mathbf{S}_{\mathrm{u}} = \left[\mathbf{a}(\theta_{\mathrm{u}1}, \varphi_{\mathrm{u}1}) \ \mathbf{a}(\theta_{\mathrm{u}2}, \varphi_{\mathrm{u}2}) \ \cdots \ \mathbf{a}\left(\theta_{\mathrm{uL_d}}, \varphi_{\mathrm{uL_d}}\right)\right]. \tag{15}$$

Corresponding to the two questions brought up in Sect. 2.3, there are two factors that affect modeling error. First, to keep the low dimensionality of propagation domain under channel training overhead constraints, only L_d dominant angles-based response vectors constructed propagation domain $\mathbf{S}_{\mathrm{d}} \in \mathbb{C}^{M \times L_d}$ is utilized for downlink channel approximation. As a result, there will still be certain channel estimation error due to the approximation; we denote this normalized channel estimation error as *approximation error*. Following the definition of normalized channel estimation error in Eq. 10, approximation error is formulated as

$$\begin{aligned} E_{\text{approximation}} &= E(\mathbf{S}_{\mathrm{d}}) \\ &= 1 - \frac{\|(\mathbf{S}_{\mathrm{d}}\mathbf{S}_{\mathrm{d}}^{\dagger}\mathbf{h}_{\mathrm{D}})^H\mathbf{h}_{\mathrm{D}}\|}{\|\mathbf{S}_{\mathrm{d}}\mathbf{S}_{\mathrm{d}}^{\dagger}\mathbf{h}_{\mathrm{D}}\|\|\mathbf{h}_{\mathrm{D}}\|}, \end{aligned} \tag{16}$$

where $\mathbf{S}_{\mathrm{d}} \in \mathbb{C}^{M \times L_d}$ is the downlink dominant propagation domain as illustrated in Eq. 14. As evident from the above equation, approximation error will be in the range from 0 to 1. When the downlink dominant propagation domain $\mathbf{S}_{\mathrm{d}} \in \mathbb{C}^{M \times L_d}$ gets closer to downlink channel in antenna domain, approximation error will decrease and get closer to 0.

Second, since downlink propagation domain information is not available before any downlink channel training, uplink channel-inferred dominant propagation domain instead of actual downlink channel dominant propagation domain is utilized for downlink channel training. Consequently, there will be extra normalized channel estimation

error due to the uplink and downlink dominant propagation domain mismatch; we denote this normalized channel estimation error as *mismatch error*, which is formulated as

$$\begin{aligned} E_{\text{mismatch}} &= E(\mathbf{S}_{\text{u}}) - E(\mathbf{S}_{\text{d}}) \\ &= \frac{\|(\mathbf{S}_{\text{d}}\mathbf{S}_{\text{d}}^{\dagger}\mathbf{h}_{\text{D}})^{H}\mathbf{h}_{\text{D}}\|}{\|\mathbf{S}_{\text{d}}\mathbf{S}_{\text{d}}^{\dagger}\mathbf{h}_{\text{D}}\|\|\mathbf{h}_{\text{D}}\|} - \frac{\|(\mathbf{S}_{\text{u}}\mathbf{S}_{\text{u}}^{\dagger}\mathbf{h}_{\text{D}})^{H}\mathbf{h}_{\text{D}}\|}{\|\mathbf{S}_{\text{u}}\mathbf{S}_{\text{u}}^{\dagger}\mathbf{h}_{\text{D}}\|\|\mathbf{h}_{\text{D}}\|}, \end{aligned} \tag{17}$$

where $\mathbf{S}_{\text{u}} \in \mathbb{C}^{M\times L_d}$ is the uplink dominant propagation domain as illustrated in Eq. 15. As evident from the above equation, mismatch error will also be in the range from 0 to 1. When the uplink channel-inferred dominant propagation domain $\mathbf{S}_{\text{u}} \in \mathbb{C}^{M\times L_d}$ gets closer to actual downlink channel one $\mathbf{S}_{\text{d}} \in \mathbb{C}^{M\times L_d}$, mismatch error will decrease and get closer to 0.

Combining approximation error and mismatch error, the total normalized error of approximating downlink channel with uplink dominant propagation domain $\mathbf{S}_{\text{u}} \in \mathbb{C}^{M\times L_d}$, i.e., modeling error, is formulated as

$$\begin{aligned} E_{\text{modeling}} &= E_{\text{approximation}} + E_{\text{mismatch}} \\ &= E(\mathbf{S}_{\text{u}}) \\ &= 1 - \frac{\|(\mathbf{S}_{\text{u}}\mathbf{S}_{\text{u}}^{\dagger}\mathbf{h}_{\text{D}})^{H}\mathbf{h}_{\text{D}}\|}{\|\mathbf{S}_{\text{u}}\mathbf{S}_{\text{u}}^{\dagger}\mathbf{h}_{\text{D}}\|\|\mathbf{h}_{\text{D}}\|}. \end{aligned} \tag{18}$$

As evident from the above equation, modeling error will be in the range from 0 to 1. When the uplink channel-inferred dominant propagation domain $\mathbf{S}_{\text{u}}$ gets closer to downlink channel in antenna domain, the modeling error will get closer to 1.

Here, we focus on modeling error in the propagation domain, while similar error analysis can be applied to other domain-based channel characterization. Also, we want to emphasize that modeling error is determined by FDD massive MIMO channel properties only and thus scheme-independent. But, modeling error is an important and necessary part to analyze and evaluate the performance of scalable FDD massive MIMO channel estimation schemes.

2.5 Performance impact

Modeling error quantifies the normalized estimation error of approximating downlink channel with uplink dominant angle response vectors. As expected, the modeling error will result in beamforming performance impact due to channel estimation error. To understand the performance impact of modeling error, here we first derive the beamforming rate loss corresponding to modeling error.

To quantify the beamforming performance impact of modeling error, as illustrated in Section 2.4, we focus on the single-user case and evaluate single-user beamforming achievable rate with conjugate beamforming. When the base-station has the perfect downlink CSI $\mathbf{h}_{\text{D}}$ available, the achievable rate with conjugate beamforming will be

$$R(\mathbf{h}_{\text{D}}, \mathbf{h}_{\text{D}}) = \mathbb{E}\left[\log\left(1 + P\|\mathbf{h}_{\text{D}}\|^2\right)\right]. \tag{19}$$

And utilizing approximated downlink channel with uplink dominant angles $\mathbf{h}_{\mathrm{uD}}$ defined as

$$\mathbf{h}_{\mathrm{uD}} = \mathbf{S}_{\mathrm{u}}\mathbf{S}_{\mathrm{u}}^{\dagger}\mathbf{h}_{\mathrm{D}}, \tag{20}$$

where $\mathbf{S}_{\mathrm{u}}$ includes uplink dominant angle response vectors as shown in Eq. 15. With conjugate beamforming, the achievable rate will be

$$R(\mathbf{h}_{\mathrm{uD}}, \mathbf{h}_{\mathrm{D}}) = \mathbb{E}\left[\log\left(1 + P\|\mathbf{h}_{\mathrm{D}}\|^2 \frac{\|\mathbf{h}_{\mathrm{uD}}^H \mathbf{h}_{\mathrm{D}}\|^2}{\|\mathbf{h}_{\mathrm{uD}}\|^2 \|\mathbf{h}_{\mathrm{D}}\|^2}\right)\right]. \tag{21}$$

Then, the rate gap between beamforming based on perfect downlink CSI $\mathbf{h}_{\mathrm{D}}$ and beamforming based on approximated downlink channel $\mathbf{h}_{\mathrm{uD}}$, denoted as *rate loss*, is formulated as

$$\begin{aligned}\Delta R &= R(\mathbf{h}_{\mathrm{D}}, \mathbf{h}_{\mathrm{D}}) - R(\mathbf{h}_{\mathrm{uD}}, \mathbf{h}_{\mathrm{D}}) \\ &= \mathbb{E}\left[\log\left(\frac{1 + P\|\mathbf{h}_{\mathrm{D}}\|^2}{1 + P\|\mathbf{h}_{\mathrm{D}}\|^2\left(1 - E_{\mathrm{modeling}}\right)^2}\right)\right].\end{aligned} \tag{22}$$

As evident from the above equation, the modeling error will affect the rate loss and larger modeling error will lead to larger rate loss.

3 Results and discussion

3.1 Modeling error: numerical results

To find out how the modeling error varies with the base-station array size, we employ the spatial channel model to investigate modeling error for the case where the base-station is equipped with a finite number of antennas. We conduct numerical simulations to observe how the modeling error varies with the number of base-station antennas and the channel angle spread. To facilitate the simulations, we set propagation domain channel parameters as follows:

- For each channel instance, both the number of clusters and the number of dominant angles for approximation are set as 4.
- Uniform distribution for the central angle of each cluster with elevation $\theta_i \sim \mathcal{U}[0^o, 180^o]$ and azimuth $\varphi_i \sim \mathcal{U}[0^o, 180^o]$.
- All clusters have the same *channel angle spread* Δ for both azimuth and elevation. In one cluster, the number of path is determined by the angle spread Δ, with all path angles uniformly sampled in elevation range $[\varphi - \Delta/2, \varphi + \Delta/2]$ and azimuth range $[\theta - \Delta/2, \theta + \Delta/2]$ with angle density as 1^o.
- All clusters have the same total power, with uniform power distribution across all the paths in each cluster: $g_{pr} = \frac{g_p}{R_p}$.

We first examine the simulation results on modeling error, as shown in Fig. 3. We investigate both the scalability with base-station array size and the dependency on channel angle spread for modeling error. Then, we examine the decomposed modeling error components, including approximation error and mismatch error, with simulation results on average error, as presented in Fig. 5. We also investigate both the scalability with

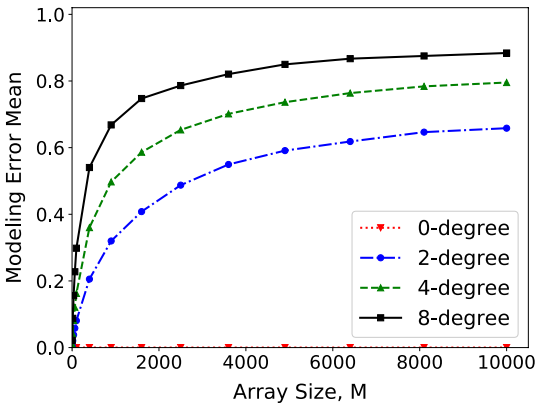

Fig. 3 Average modeling error changes with the number of base-station antennas. The plot is based on *simulated* channels with different angle spreads, respectively

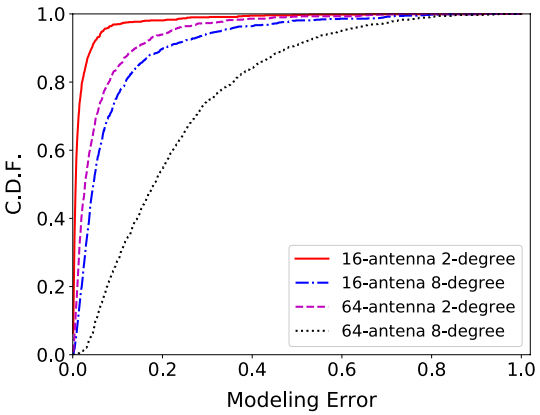

Fig. 4 The cumulative distribution function of modeling error with two different array sizes. The plot is based on *simulated* channels with different angle spreads, respectively

base-station array size and the dependency on channel angle spread for both approximation error and mismatch error. All the numerical results are based on 10, 000 simulated independent channel instances.

Observation 1—Modeling Error Increases with Both Base-station Array Size and Channel Angle Spread: In terms of the scalability with base-station array size, we observe that the average modeling error increases with the number of base-station antennas, from Fig. 3. For example, when the channel angle spread is 2-degree, the average modeling error increases from 0.02 with 16 antennas, to 0.06 with 64 antennas, and to 0.65 with 10, 000 antennas. The same trend is also observed in Fig. 4 with the cumulative distribution function of modeling error, which shows that more base-station antennas lead to larger modeling error. In terms of the dependency on channel angle spread, we observe that larger angle spread will result in larger average modeling error, from Fig. 3. For example, when the base-station is equipped with 64 antennas, the average modeling error increases from 0 with 0-degree angle spread, to 0.06 with 2-degree angle spread and to 0.23 with 8-degree angle spread. The same trend is also observed in Fig. 4 with the cumulative distribution function of modeling error, which shows that larger channel angle spread results in larger modeling error.

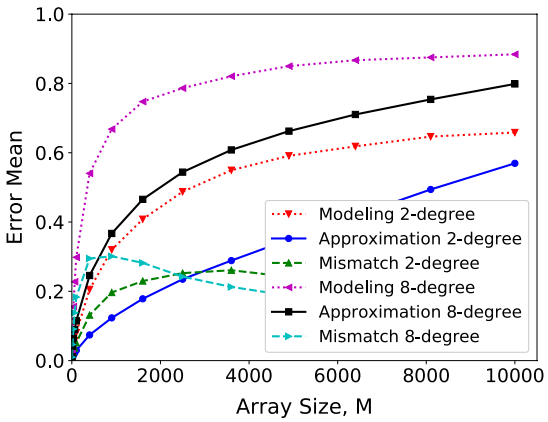

Fig. 5 Modeling error decomposed to approximation error and mismatch error changing with base-station array size. The plot is based on *simulated* channels with different angle spreads, respectively

Explanation for Observation 1: Modeling error quantifies the normalized error of approximating downlink channel with a fixed number of uplink dominant angle response vectors. For the scalability with base-station array size, since the array beamwidth is inversely proportional to the number of base-station antennas, the captured relative channel power with a fixed number of dominant angle response vectors will get smaller when the base-station is equipped with more antennas. As a result, modeling error increases with the base-station array size. For the dependency on channel angle spread, since larger channel angle spread indicates more distributed channel power, a fixed number of dominant angle response vectors will capture less channel power when the channel angle spread gets larger. Consequently, modeling error increases with the channel angle spread.

Observation 2—Approximation Error Increases with Both Base-station Array Size and Channel Angle Spread: As shown in Fig. 5, the average approximation error increases with the number of base-station antennas. For example, when the channel angle spread is 2-degree, the average approximation error increases from 0.01 with 16 antennas, to 0.02 with 64 antennas and to 0.6 with 10, 000 antennas. And larger angle spread will result in more approximation error, from 0.02 when angle spread is 2-degree to 0.09 when angle spread is 8-degree with 64-antenna at the base-station.

Explanation for Observation 2 Approximation error quantifies the normalized error of approximating downlink channel with a fixed number of dominant angle response vectors instead of all angle response vectors. For both the scalability with base-station array size and the dependency on channel angle spread, the reasons are the same ones as in the explanation for Observation 1.

Observation 3—Mismatch Error First Increases Then Decreases with Base-station Array Size and Larger Channel Angle Spread Leads to More Mismatch Error As shown in Fig. 5, the average mismatch error first increases and then decreases with the number of base-station antennas. For example, when the channel angle spread is 8-degree, the average mismatch error increases from 0.04 with 16 antennas, to 0.3 with 400 antennas, and then drops to 0.08 with 10, 000 antennas. Also, larger channel angle spread will result in larger mismatch error, from 0.04 when angle spread is 2-degree to 0.14 when angle spread is 8-degree with 64-antenna at the base-station.

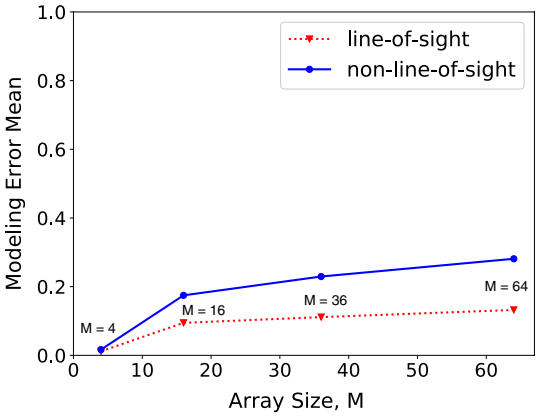

Fig. 6 Average modeling error changing with the number of base-station antennas. The plot is based on *measured* line-of-sight and non-line-of-sight channels, respectively

Explanation for Observation 3 Mismatch error quantifies the normalized error gap between approximated downlink channel with uplink dominant angle response vectors and approximated downlink channel with downlink dominant angle response vectors. For the scalability with the base-station array size, due to uplink/downlink dominant angles difference resulting from channel phase parameters difference, the captured normalized channel power by uplink dominant angle response vectors decreases at a larger rate than that by downlink dominant angle response vectors when the number of base-station antennas increases. As a result, mismatch error first increases and then decreases with the base-station array size. For the dependency on channel angle spread, the reason is the same one as in the explanation for Observation 1.

3.2 Modeling error: experimental results

To further validate the observations on modeling error from numerical results, here we investigate modeling error based on measured FDD massive MIMO channels as detailed in Sect. 2.2. We take the measured FDD massive MIMO channels as input to evaluate modeling error. Similar to numerical results, we examine the scalability with base-station array size and the dependency on channel angle spread for modeling error, and the results are shown in Figs. 6 and 7.

Finding 1—Modeling error Increases with Base-station Array Size and Non-Line-of-sight Channels Yield Larger Modeling error Than Line-of-sight Channels In terms of the scalability with base-station array size, we find out that the average modeling error increases with the number of base-station antennas from Fig. 6. For example, for non-line-of-sight channels, the average modeling error increases from 0.02 with 4 antennas, to 0.18 with 16 antennas, and to 0.28 with 64 antennas. The same trend is also observed in Fig. 7 with the cumulative distribution function of modeling error, which shows that more base-station antennas always lead to smaller modeling error. When comparing line-of-sight channels with non-line-of-sight channels, we find out that non-line-of-sight channels result in larger average modeling error than line-of-sight channels from Fig. 6. For example, when the base-station is equipped with 64 antennas, the average modeling error of non-line-of-sight channels is 0.28, which is larger than the average modeling error 0.13 of line-of-sight channels. The same finding is also obtained from Fig. 7 with the cumulative distribution function of modeling error.

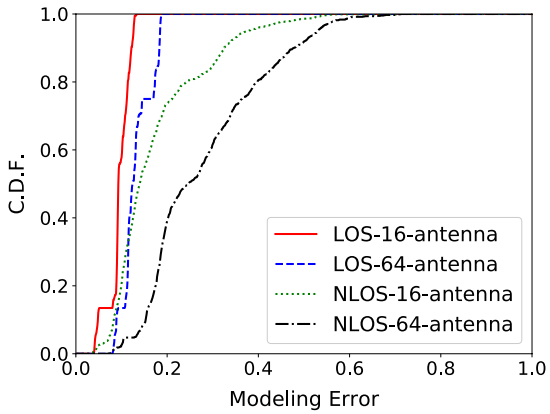

Fig. 7 Cumulative distribution function of modeling error with two different array sizes. The plot is based on *measured* line-of-sight and non-line-of-sight channels, respectively

Explanation for Finding 1: For the scalability with base-station array size, the finding matches numerical Observation 1. For the comparison between line-of-sight channels and non-line-of-sight channels, since non-line-of-sight channels exhibit more distributed channel power over angles than line-of-sight channels, a fixed number of dominant angles will capture less channel power for non-line-of-sight channels. When comparing measured channels to simulated channels, line-of-sight channels have a smaller channel angle spread than non-line-of-sight channels. Therefore, for the dependency on channel angle spread, the experimental finding also matches numerical Observation 3.

3.3 Performance impact: numerical results

To understand the performance impact of modeling error, we first employ the spatial channel model to investigate rate loss. Here as illustrated in Sect. 2.4, we focus on the single-user case and evaluate single-user beamforming achievable rate with conjugate beamforming. We conduct numerical simulations to observe how the rate loss varies with the number of base-station antennas and the channel angle spread.

Observation 4—Rate Loss Increases with Both Base-station Array Size and Channel Angle Spread The simulation results on rate loss are shown in Fig. 8. In terms of the scalability with base-station array size, we observe that rate loss increases with the number of base-station antennas, from Fig. 8. For example, when the channel spread is 2 degrees, rate loss increases from 0.1 bps/Hz with 4 antennas, to 0.25 bps/Hz with 64 antennas, and to 3 bps/Hz with 10, 000 antennas. In terms of the dependency on channel angle spread, we observe that larger angle spread will result in larger rate loss, from Fig. 8. For example, when the base-station is equipped with 64 antennas, rate loss increases from 0 bps/Hz with 0-degree angle spread, to 0.25 bps/Hz with 2-degree angle spread, and to 1 bps/Hz with 8-degree angle spread.

Explanation for Observation 4: We explain the observation based on the relationship between rate loss and modeling error as shown in Eq. 22. Since modeling error decreases with the base-station array size, as shown in Observation 1, accordingly, rate loss power decreases with the base-station array size. And since larger channel angle spread leads to smaller modeling error, accordingly, rate loss decreases with the channel angle spread.

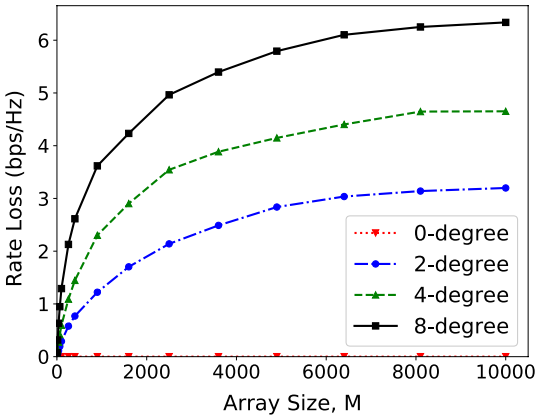

Fig. 8 Rate loss changing with base-station array size. The plot is based on *simulated* channels with different angle spreads

3.3.1 Performance impact: experimental results

To further validate the observation of rate loss from numerical results, we also investigate the rate loss based on measured FDD massive MIMO channels. Again, we focus on the single-user case and evaluate single-user beamforming achievable rate with conjugate beamforming. Similar to numerical results, we examine the scalability with the base-station array size and the dependency on the channel angle spread for the rate loss.

Finding 2—Rate Loss Increases with Base-station Array Size and Line-of-sight Channels Yield Smaller Rate Loss Than Non-line-of-sight Channels The experimental results on rate loss are shown in Fig. 10. In terms of the scalability with base-station array size, we observe that rate loss increases with the number of base-station antennas, from Fig. 11. For example, for line-of-sight channels, rate loss increases from 0.03 bps/Hz with 4 antennas to 0.4 bps/Hz with 64 antennas. When comparing line-of-sight channels with non-line-of-sight channels, we find out that line-of-sight channels result in smaller rate loss than non-line-of-sight channels from Fig. 6a. For example, when the base-station is equipped with 64 antennas, rate loss of line-of-sight channels is 0.4 bps/Hz, which is smaller than rate loss 1 bps/Hz of non-line-of-sight channels.

Explanation for Finding 2 For the scalability with base-station array size, the finding matches numerical Observation 4. For the comparison between line-of-sight channels and non-line-of-sight channels, since non-line-of-sight channels exhibit more distributed channel power over angles than line-of-sight channels, a fixed number of dominant angles will capture less channel power for non-line-of-sight channels. When comparing measured channels with simulated channels, line-of-sight channels have a smaller channel angle spread than non-line-of-sight channels. Therefore, for the dependency on channel angle spread, the experimental finding also matches numerical Observation 4.

Combining the numerical observation with the experimental finding, we find out that even though modeling error leads to rate loss that increases with the number of base-station antennas, more base-station antennas still bring in more beamforming performance improvement with estimated downlink channel, as shown in both Fig. 9 and Fig. 11. Therefore, we can conclude that taking the modeling error into account, scalable channel estimation schemes that exploit the propagation domain,

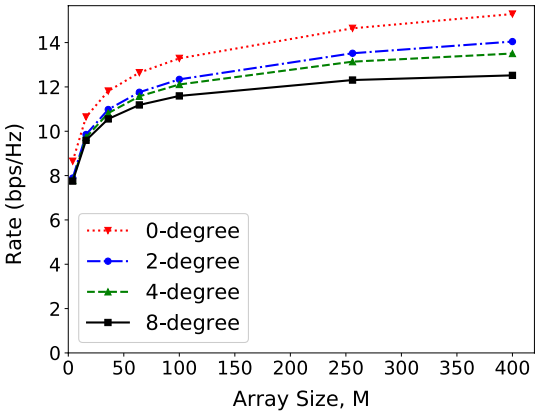

Fig. 9 Beamforming rate with approximated downlink channel changing with base-station array size. The plot is based on *simulated* channels with different angle spreads

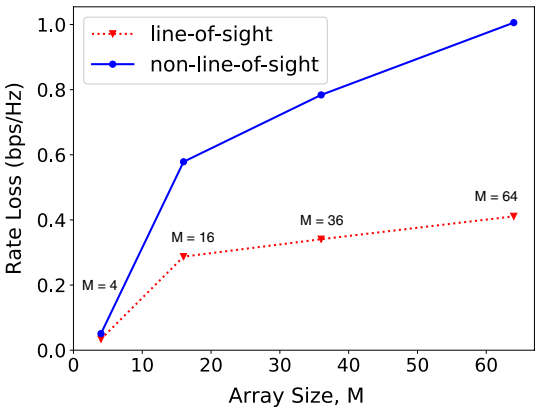

Fig. 10 Rate loss changing with base-station array size. The plot is based on *measured* channels

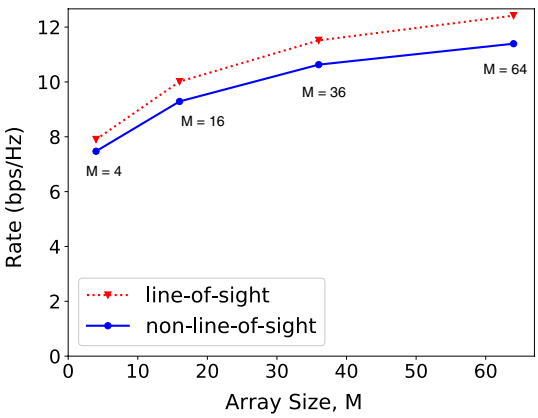

Fig. 11 Beamforming rate with approximated downlink channel changing with base-station array size. The plot is based on *measured* channels

e.g., directional training in [26], can still benefit from the array gain and bring in beamforming performance improvement in the massive MIMO regime.

4 Conclusion

Inspired by the experimental findings on channel propagation domain properties, we first formulate modeling error to quantify the normalized estimation error of approximating downlink channel with uplink dominant angles. From our analysis and numerical results, we observe that modeling error increases with the number of base-station antennas, and more distributed power channels lead to larger modeling error. We also validate the observation by experimental results.

Then, we investigate the performance impact of modeling error and quantify the resulting downlink beamforming rate loss of approximating downlink channel with uplink dominant angles. From both numerical and experimental results, we observe that the rate loss increases with the number of base-station antennas, and more distributed power channels will result in larger rate loss. Also, even though the rate loss increases with the number of base-station antennas, we find out the beamforming rate still increases with array size. Based on the observation, we conclude that beamforming based on scalable channel estimation schemes that exploit the propagation domain, e.g., directional training in [26], benefits from the array gain in FDD massive MIMO.

In this paper, we mainly focus on channel in the propagation domain with angle response vectors characterization and investigate the corresponding modeling error, along with the beamforming performance impact. However, similar error analysis can be conducted for alternate channel characterizations. Also, our analysis will be an important part to help improve FDD channel estimation schemes and other related applications. A detailed example is to optimize time resources allocated to downlink channel training during channel estimation, where there is a trade-off between training overhead and channel estimation error.

Abbreviations

FDD	Frequency-division duplexing
MIMO	Multi-input multi-output
CSI	Channel state information
OFDM	Orthogonal frequency-division multiplexing
3GPP	Third-generation partnership project

Acknowledgements
Not applicable.

Author Contributions
The authors contributed equally. Both the authors have read and approved the final version of the manuscript.

Funding
The authors were partially supported by NSF grant 1518916 and support from Qualcomm, Inc.

Availability of data and materials
Not applicable.

Declarations

Competing interests
The authors declare that they have no competing interests.

Received: 21 April 2021 Accepted: 30 November 2022
Published online: 16 March 2023

References

1. T.L. Marzetta, Noncooperative cellular wireless with unlimited numbers of base station antennas. IEEE Trans. Wirel. Commun. **9**(11), 3590–3600 (2010)
2. E.G. Larsson, O. Edfors, F. Tufvesson, T.L. Marzetta. Massive MIMO for next generation wireless systems. arXiv:1304.6690 (2013)
3. F. Rusek, D. Persson, B.K. Lau, E.G. Larsson, T.L. Marzetta, O. Edfors, F. Tufvesson, Scaling up MIMO: opportunities and challenges with very large arrays. IEEE Signal Process. Mag. **30**(1), 40–60 (2013)
4. H.Q. Ngo, E.G. Larsson, T.L. Marzetta, Energy and spectral efficiency of very large multiuser MIMO systems. IEEE Trans. Commun. **61**(4), 1436–1449 (2013)
5. C. Shepard, H. Yu, N. Anand, E. Li, T. Marzetta, R. Yang, L. Zhong. Argos: Practical many-antenna base stations, in Proceedings of the 18th Annual International Conference on Mobile Computing and Networking, pp. 53–64 (2012). ACM
6. C.-S. Lee, M.-C. Lee, C.-J. Huang, T.-S. Lee. Sectorization with beam pattern design using 3D beamforming techniques, in 2013 Asia-Pacific Signal and Information Processing Association Annual Summit and Conference, pp. 1–5 (2013). IEEE
7. X. Cheng, B. Yu, L. Yang, J. Zhang, G. Liu, Y. Wu, L. Wan, Communicating in the real world: 3D MIMO. IEEE Wirel. Commun. **21**(4), 136–144 (2014)
8. L. You, X. Gao, X.-G. Xia, N. Ma, Y. Peng, Pilot reuse for massive MIMO transmission over spatially correlated rayleigh fading channels. IEEE Trans. Wirel. Commun. **14**(6), 3352–3366 (2015)
9. H. Xie, F. Gao, S. Zhang, S. Jin, A unified transmission strategy for TDD/FDD massive MIMO systems with spatial basis expansion model. IEEE Trans. Veh. Technol. **66**(4), 3170–3184 (2016)
10. P. Patcharamaneepakorn, S. Wu, C.-X. Wang, M.M. Alwakeel, X. Ge, M. Di Renzo, Spectral, energy, and economic efficiency of 5G multicell massive MIMO systems with generalized spatial modulation. IEEE Trans. Veh. Technol. **65**(12), 9715–9731 (2016)
11. N. Garcia, H. Wymeersch, E.G. Larsson, A.M. Haimovich, M. Coulon, Direct localization for massive MIMO. IEEE Trans. Signal Process. **65**(10), 2475–2487 (2017)
12. X. Du, A. Sabharwal. Shared angles-of-departure in massive MIMO channels: Correlation analysis and performance impact. submitted to IEEE Transactions on Wireless Communications (2019)
13. X. Du, Y. Sun, N. Shroff, A. Sabharwal, Balance queueing and retransmission: Latency-optimal massive MIMO design. arXiv:1902.07676 (2019)
14. A. Adhikary, J. Nam, J.-Y. Ahn, G. Caire, Joint spatial division and multiplexing-the large-scale array regime. IEEE Trans. Inform. Theory **59**(10), 6441–6463 (2013)
15. W. Shen, L. Dai, B. Shim, S. Mumtaz, Z. Wang, Joint CSIT acquisition based on low-rank matrix completion for FDD massive MIMO systems. IEEE Commun. Lett. **19**(12), 2178–2181 (2015)
16. Z. Gao, L. Dai, Z. Wang, S. Chen, Spatially common sparsity based adaptive channel estimation and feedback for FDD massive MIMO. IEEE Trans. Signal Process. **63**(23), 6169–6183 (2015)
17. X. Zhang, J. Tadrous, E. Everett, F. Xue, A. Sabharwal, Angle-of-arrival based beamforming for FDD massive MIMO, in 2015 49th Asilomar Conference on Signals, Systems and Computers, pp. 704–708 (2015). IEEE
18. Z. Jiang, A.F. Molisch, G. Caire, Z. Niu, Achievable rates of FDD massive MIMO systems with spatial channel correlation. IEEE Trans. Wirel. Commun. **14**(5), 2868–2882 (2015)
19. J. Fang, X. Li, H. Li, F. Gao, Low-rank covariance-assisted downlink training and channel estimation for FDD massive MIMO systems. IEEE Trans. Wirel. Commun. **16**(3), 1935–1947 (2017)
20. D. Fan, F. Gao, G. Wang, Z. Zhong, A. Nallanathan, Angle domain signal processing-aided channel estimation for indoor 60-ghz TDD/FDD massive MIMO systems. IEEE J. Sel. Areas Commun. **35**(9), 1948–1961 (2017)
21. H. Xie, F. Gao, S. Jin, J. Fang, Y.-C. Liang, Channel estimation for TDD/FDD massive MIMO systems with channel covariance computing. IEEE Trans. Wirel. Commun. **17**(6), 4206–4218 (2018)
22. M.B. Khalilsarai, S. Haghighatshoar, X. Yi, G. Caire, FDD massive MIMO via UL/DL channel covariance extrapolation and active channel sparsification. IEEE Trans. Wirel. Commun. **18**(1), 121–135 (2018)
23. Y. Han, Q. Liu, C.-K. Wen, M. Matthaiou, X. Ma, Tracking fdd massive mimo downlink channels by exploiting delay and angular reciprocity. IEEE J. Sel. Top. Signal Process. **13**(5), 1062–1076 (2019)
24. F. Rottenberg, T. Choi, P. Luo, C.J. Zhang, A.F. Molisch, Performance analysis of channel extrapolation in fdd massive mimo systems. IEEE Trans. Wirel. Commun. **19**(4), 2728–2741 (2020)
25. B. Banerjee, R.C. Elliott, W.A. Krzymień, H. Farmanbar, Towards fdd massive mimo: Downlink channel covariance matrix estimation using conditional generative adversarial networks, in 2021 IEEE 32nd Annual International Symposium on Personal, Indoor and Mobile Radio Communications (PIMRC), pp. 940–946 (2021). IEEE
26. X. Zhang, L. Zhong, A. Sabharwal, Directional training for FDD massive MIMO. IEEE Transactions on Wireless Communications (2018)
27. 3GPP: Study on 3D channel model for LTE. TR 36.873, 3rd Generation Partnership Project (3GPP) (2015). http://www.3gpp.org/dynareport/36873.htm

Publisher's Note